

Article

Flood Risk Assessment Using TELEMAC-2D Models Integrated with Multi-Index Analysis in Shenzhen River Basin, China

Guoyi Li ^{1,*}, Jiahong Liu ^{1,2,*}  and Weiwei Shao ¹ 

¹ State Key Laboratory of Simulation and Regulation of Water Cycle in River Basin, China Institute of Water Resource and Hydropower Research, Beijing 100038, China

² Water Resources and Water Ecological Engineering Technology Research Center of Ministry of Water Resources, Beijing 100044, China

* Correspondence: liguoyi0701@163.com (G.L.); liujh@iwhr.com (J.L.)

Abstract: An urban flood simulation model based on TELEMAC-2D was constructed, and the inundation data of two measured rainstorms (7 June 2018 and 16 September 2018) were selected to validate the model. Flooding processes were simulated under 12 designed rainfall scenarios with rainfall return periods of 20, 50 and 100 years and rainfall peak coefficients of 0.2, 0.4, 0.6 and 0.8, respectively. The hazard-vulnerability (H-V) method was used for urban flood risk assessment. The selected hazard factors included inundation depth, flood velocity, elevation and slope. The vulnerability factors included land use type, population density and property distribution. The analytic hierarchy process (AHP) method was used to calculate the weight values of each indicator factor, and ArcGIS software was used for overlay calculation. The results of the analysis show that as the rainfall peak coefficient factor increases, the area of each risk zone increases to varying degrees. The larger the rainfall peak coefficient factor, the more serious the flooding. As the rainfall return period increases, the effect of the rainfall peak coefficient factor of the change in the area of the highest risk zone diminishes. The highest risk zone is the largest within Luohu District (LHD), accounting for 46.38%, 60.92% and 45.54% of the total highest risk area, respectively. As the return period increases, the area of the highest risk zone within Futian District (FTD) increases, but its proportion has a decreasing trend, and the proportion of the highest risk area within Longgang District (LGD) has an increasing trend. The risk zoning map can better reflect the risk distribution of the basin and provide a scientific basis for early warning of flood prevention and drainage in the Shenzhen River basin.

Keywords: urban flood disaster; TELEMAC-2D model; analytic hierarchy process; indicator system method; flood risk assessment



Citation: Li, G.; Liu, J.; Shao, W. Flood Risk Assessment Using TELEMAC-2D Models Integrated with Multi-Index Analysis in Shenzhen River Basin, China. *Water* **2022**, *14*, 2513. <https://doi.org/10.3390/w14162513>

Academic Editor: Maria Mimikou

Received: 11 July 2022

Accepted: 11 August 2022

Published: 15 August 2022

Publisher's Note: MDPI stays neutral with regard to jurisdictional claims in published maps and institutional affiliations.



Copyright: © 2022 by the authors. Licensee MDPI, Basel, Switzerland. This article is an open access article distributed under the terms and conditions of the Creative Commons Attribution (CC BY) license (<https://creativecommons.org/licenses/by/4.0/>).

1. Introduction

Many countries face serious threats due to the increased frequency and intensity of extreme weather events (typhoons, heat waves, floods) affected by global climate change [1]. According to estimates by experts from the World Bank, the average annual flood losses in 136 mega coastal cities in the world in 2005 were about USD 6 billion, and it is expected that this value will increase to USD 52 billion by 2050 [2]. Climate change and urbanization continue to accelerate, resulting in widespread casualties and economic losses and seriously threatening the normal functioning of urban social activities [3–5]. According to statistics, the losses caused by rainstorms and floods account for 40% of the total losses from various natural disasters worldwide [6]. From 1998 to 2017, over 170 countries and more than 2 billion people worldwide were affected by heavy rainfall and flooding and caused economic losses of up to USD 656 billion [7]. In its series of reports, the IPCC 5th has identified extreme rainfall due to global climate change as one of the main influences on the frequency of rainfall and flooding [8]. China is one of the regions with frequent rainstorms and floods. Until 2020, China's urbanization rate exceeded 60% [9]. Urbanization has changed the type

of underlying surface in the original area, resulting in a significant increase in the area of impervious areas and a consequent increase in the risk of urban flooding [10]. According to the statistics of China's housing and construction department, from 2008 to 2010, 213 cities in China experienced waterlogging of varying degrees, and 137 cities suffered from waterlogging disasters more than three times [11]. In recent years, phenomena such as "cities looking at the sea" and "cities looking at rivers" have frequently occurred, and urban flooding disasters have received widespread attention.

The definition of flood risk is not unique; it is mainly defined as the product of hazard, exposure and vulnerability [12–16]. In recent years, on a global scale, urban flood risk assessment has become a hot issue in disaster control and management [17,18]. Scholars have carried out a great deal of research on the analysis of urban flooding hazards [19,20]. Yashon O. Ouma et al. used the technology combining AHP and GIS (Geographic Information System) to analyze the flood risk in Eldoret Municipality in Kenya and draw a flood analysis map [21]. Liu Jiahong et al. delved into the basis of sponge city flood control, using Tongzhou, Beijing as the study area, and introduced the GAUSS function for nonlinear fitting to study the flood control mechanism of sponge city flood control system [22]. Binh Thai Pham et al. took Quang Nam Province, Vietnam, as a study area and used deep learning methods to evaluate the urban flood risk in the region [23,24]. Xinxiang Lei et al. adopted the deep learning approach and selected several different influencing factors to analyze the urban flood risk in Seoul, South Korea [14]. Y. Budiyo et al. [25] and Foudi et al. [26] provided a comprehensive consideration of the impact of hazards, exposure and vulnerability on flood risk assessment and risk assessment at global and local scales. Zhihui Li et al. provided an analytical assessment of urban flooding processes in Wuhan, China, based on analytic hierarchy process, considering land use and climate change [27]. The index system approach is one of the commonly used risk analysis methods, which is widely used and highly adaptable; the flood risk assessment method based on scenario simulation can achieve dynamic assessment of flood hazards by setting up rainfall simulation models and setting up different rainfall scenarios [28].

In this paper, combining the advantages of the scenario simulation method and the index system approach, taking the SRB (Shenzhen River Basin) in Shenzhen as the research area, the following research work is carried out:

- (i) Constructing an urban flooding simulation model based on the TELEMAC-2D two-dimensional hydrodynamic model, simulating the urban flooding process under 12 different design rainfall scenarios, and analysing the evolution of the hazard factors such as inundation depth, inundation area and flood velocity;
- (ii) By extracting the inundation depth and flow velocity values calculated by the flood simulation model, and considering factors such as elevation, slope, land use type, population density and property distribution, the AHP method was used to calculate the weight values of different influencing factors, and the H-V method was used to assess the flood risk in the study area. The study area was classified into different flood risk classes;
- (iii) Analysis of flood risk delineation maps, statistical analysis of the distribution of risk levels under different rainfall scenarios and analysis of inundation within different administrative districts within different catchments.

Section 2 provides a detailed introduction to the research area and introduces the research method and acquisition and pre-treatment of data. Section 3 analyzes the flood risk assessment results in the study area. Section 4 discusses the main contributions, drawbacks and issues to be addressed in the next step. Section 5 summarizes the main conclusions.

2. Materials and Methods

2.1. Study Area

Shenzhen (113°43'–114°38' E, 22°24'–22°55' N) has a subtropical oceanic climate with a mild climate, with an average annual temperature of 22.4 °C and average annual

precipitation of 1830 mm. The spatial distribution of rainfall is uneven, with more in the southeast and less in the northwest, showing a phenomenon of decreasing from east to west. The eastern region is about 2000 mm, the central area is 1700–2000 mm, and the western area is about 1700 mm. The precipitation time distribution in the city is uneven, and the precipitation is mainly concentrated in the flood season from April to October, accounting for about 85% of the annual precipitation. Due to the uneven spatial and temporal distribution of precipitation, droughts and floods often occur alternately. Shenzhen is a special economic zone in China, a national economic center city and an international city approved by the State Council. Shenzhen has 9 administrative districts and 1 new district, with a total area of 1997.47 km², of which 927.96 km² are built-up areas and resident populations. It has reached 13.4388 million people, and the urbanization rate is 100%, making it the first fully urbanized city in China. In 2020, the GDP of Shenzhen will be 2767.024 billion yuan. Shenzhen is located on the southeast coast of China and is affected by typhoons and rainstorms every year, resulting in urban waterlogging. For instance, in 2018, Super Typhoon Mangkhut was one of the strongest typhoons in Shenzhen's history, causing heavy rain in the city. In 2020, Typhoon Higos hit Shenzhen, and the maximum rainfall in Shenzhen reached 205.3 mm. The heavy rainfall brought by these typhoons has caused various degrees of waterlogging in Shenzhen, causing serious social impacts. In this study, the SRB in Shenzhen is selected as the research area. The research area includes LHD, FTD (portion) and LGD (portion) of Shenzhen City, which is an economically developed and densely populated area [29]. Once the SRB suffers from rainstorms and waterlogging disasters, it will cause great economic loss and social impact. The location of the study area is shown in Figure 1.

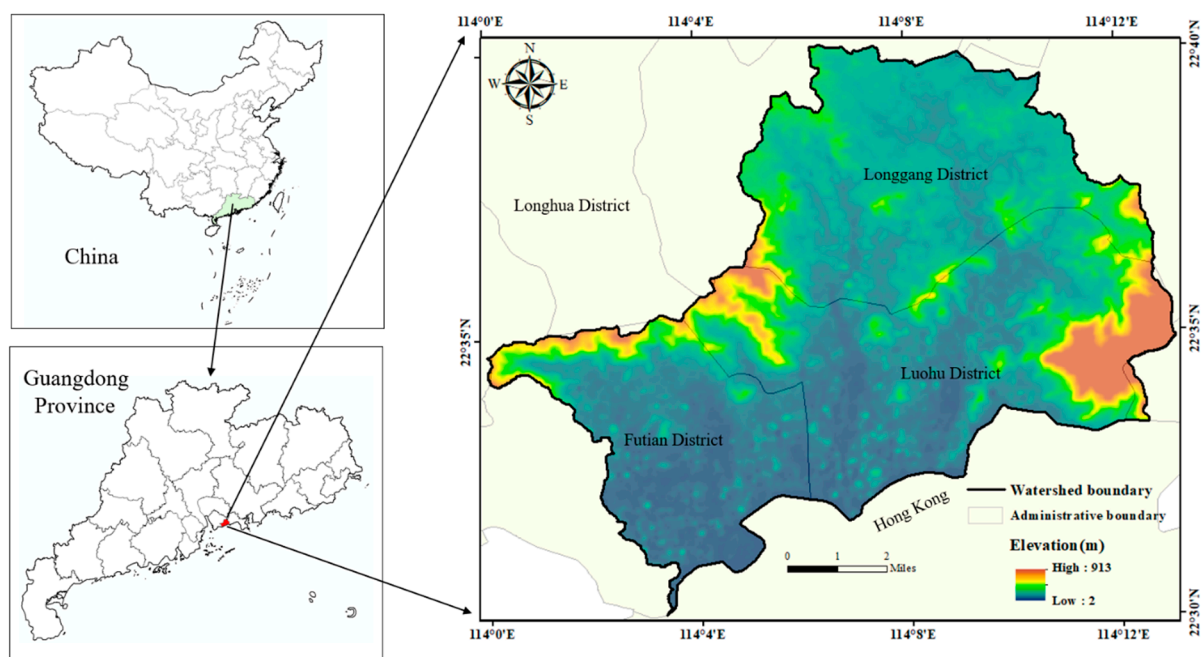


Figure 1. Location and Shenzhen River Basin.

2.2. Research Methods

In this study, the H-V method [30] was adopted to assess the flood risk of the SRB in Shenzhen, as shown in Figure 2. The urban flood disaster was considered a comprehensive function of hazard and vulnerability. Referring to the relevant literature, the disaster risk expression of the H-V method is shown in Equation (1). After the flood risk index is determined, the weight of each index should be calculated. The AHP method is widely used in flood risk assessment, especially for urban scale flood risk assessment [31]. In the 1970s, American operations researcher T.L. Saaty proposed the analytic hierarchy

process (AHP), which is a multi-level weighting analysis of decision-making methods, a combination of qualitative and quantitative systems analysis [32,33]. The AHP to determine the indicator weights includes the following four calculation steps: (1) establishing the hierarchical structure model; (2) constructing the judgment matrix; (3) calculating the indicator weight values; (4) and conducting consistency tests. When $CR < 0.1$, it can be considered that the judgment matrix passes the consistency test, and the weight values are reasonable. Otherwise, the consistency test needs to be conducted again. In this study, the flood risk assessment system was constructed according to the object layer, index layer and indicator layer. When the CR values were less than 0.1, the results obtained were reliable and reasonable through the consistency test. The obtained weight values of each indicator are shown in the Tables 1 and 2.

$$R = x_H \left(\sum_{i=1}^n H_i h_i \right) \times x_V \left(\sum_{j=1}^n V_j v_j \right) \tag{1}$$

where R is the urban flood disaster risk, x_H and x_V are the weight values of the hazard and vulnerability indicators, H_i and V_j are specific indicator factors, and h_i and v_j are the weight values of each specific index factor.

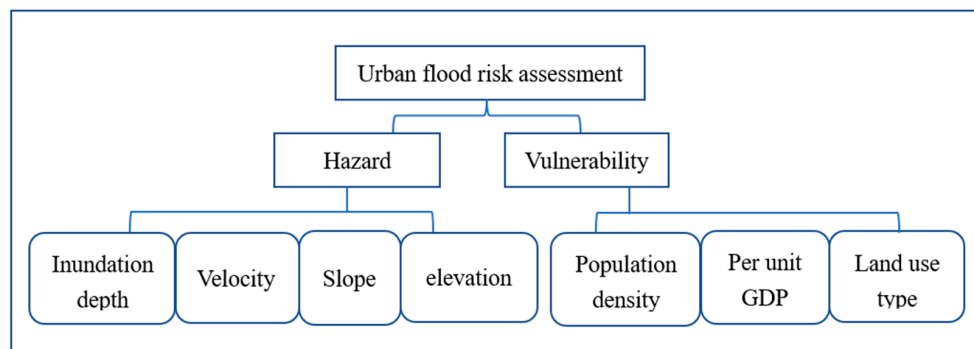


Figure 2. Flood risk assessment indicator system of Shenzhen River basin.

Table 1. Selected index factors and relative weight.

Object Layer	Index Layer	Relative Weight	Indicator Layer	Relative Weight
Flood risk assessment	Hazard	0.67	Depth	0.46
			Velocity	0.27
			Elevation	0.19
			Slope	0.08
	Vulnerability	0.33	Population density	0.54
			Per unit GDP	0.30
			Land use	0.16

Table 2. Comparison matrix for urban flood risk assessment.

Comparison Matrix for Hazard Indicators					
	Depth	Velocity	Elevation	Slope	Relative Weight
Depth	1	2	3	4	0.46
Velocity	1/2	1	2	3	0.276
Elevation	1/3	1/2	1	4	0.19
Slope	1/4	1/3	1/4	1	0.08

Comparison Matrix for Vulnerability Indicators				
	Population Density	Per Unit GDP	Land use	Relative Weight
Population density	1	2	3	0.54
Per unit GDP	1/2	1	2	0.30
Land use	1/3	1/2	1	0.16

Note: $\lambda = 4.15$, $CR = 0.057 < 0.1$, passing the consistency verification. $\lambda = 3$, $CR = 0.0089 < 0.1$, passing the consistency verification.

In this paper, TELEMAC-2D was used to conduct a two-dimensional hydrodynamic simulation of urban waterlogging. The TELEMAC-2D model is a two-dimensional module in the TELEMAC-MASCARET model developed by the French National Laboratory for Hydraulics and Environment. The TELEMAC-2D model is widely used in coastal and other large-scale storm surge simulations, but there are few studies on urban flood simulation. The article uses the v7p2r3 version for urban flood simulation, and the model uses the finite element method to solve the non-conservative two-dimensional shallow water equation, which can be calculated as follows:

$$\frac{\partial h}{\partial t} + \frac{\partial(hu)}{\partial x} + \frac{\partial(hv)}{\partial y} = 0 \tag{2}$$

$$\frac{\partial u}{\partial t} + u \frac{\partial u}{\partial x} + v \frac{\partial u}{\partial y} = -g \frac{\partial Z}{\partial x} + F_x + \frac{1}{h} \text{div}(hv_e \nabla u) \tag{3}$$

$$\frac{\partial v}{\partial t} + u \frac{\partial v}{\partial x} + v \frac{\partial v}{\partial y} = -g \frac{\partial Z}{\partial y} + F_y + \frac{1}{h} \text{div}(hv_e \nabla v) \tag{4}$$

where h is the water depth (m), Z is the free surface elevation (m), u and v are the velocity components (m/s), t is the time (s), g is the gravity acceleration (m^2/s), x and y are the horizontal space coordinates (m), v_e is the coefficient of viscosity, and F_x and F_y are the bottom bed friction coefficients.

The SCS-CN (soil conservation service) rainfall-runoff model is an empirical model proposed by the Soil Conservation Department of the United States in 1954. The model is derived from the rainfall and runoff data of small watersheds in different regions. The SCS-CN infiltration model in the United States is used in TELEMAC-2D. The calculation formula of the SCS model is as follows:

$$Q = \frac{(P - I_a)^2}{(P - I_a) + S} \tag{5}$$

$$I_a = 0.2S \tag{6}$$

$$Q = \frac{(P - 0.2S)^2}{(P + 0.8S)} \tag{7}$$

$$S = \frac{1000}{CN} - 10 \tag{8}$$

where Q is the runoff (m^3), P is the precipitation (mm), I_a is the initial abstraction (mm), and the CN (curve number) value can be determined by an empirical value table.

The TELEMAC-2D two-dimensional hydrodynamic model was used for urban flood analysis, and the BlueKenue 64 software was used to divide the study area into nonlinear triangular meshes with a total of 240,570 nodes and 477,797 meshes. The boundary conditions of the model are free outflow boundary conditions, and the Courant number is 0.75. Considering that Shenzhen is located in the southeastern coastal area of China, the climate is humid and rainy, and referring to the research results in similar areas [34,35], the soil water content in the early stage is set to AMC-II (the soil moisture condition was moderate). The duration of this flood simulation is 6 h, and the time step is 0.5 s. The relevant parameter values are shown in Tables 3 and 4. The properties of the underlying surface in the study area are shown in Figure 3.

Table 3. CN value.

Land Use	B	C	D
Buildings	90	92	94
Road	98	98	98
Bare	83	88	90
Green	61	74	80
Water	98	100	100
Others	80	88	97

Note: B is silt loam or loam, with good permeability; C is sandy clay loam, with medium permeability; D is clay loam, silty clay loam, sandy clay, silty clay, or clay, with poor permeability. The CN value is determined according to the World Soil Database and the American SCS Model Soil Classification Standard.

Table 4. Manning coefficient.

Land Use	Buildings	Road	Bare	Green	Water	Others
n	0.2	0.05	0.065	0.08	0.015	0.05

Note: The Manning coefficients are grouped according to the land use type and soil hydrology in the study area.

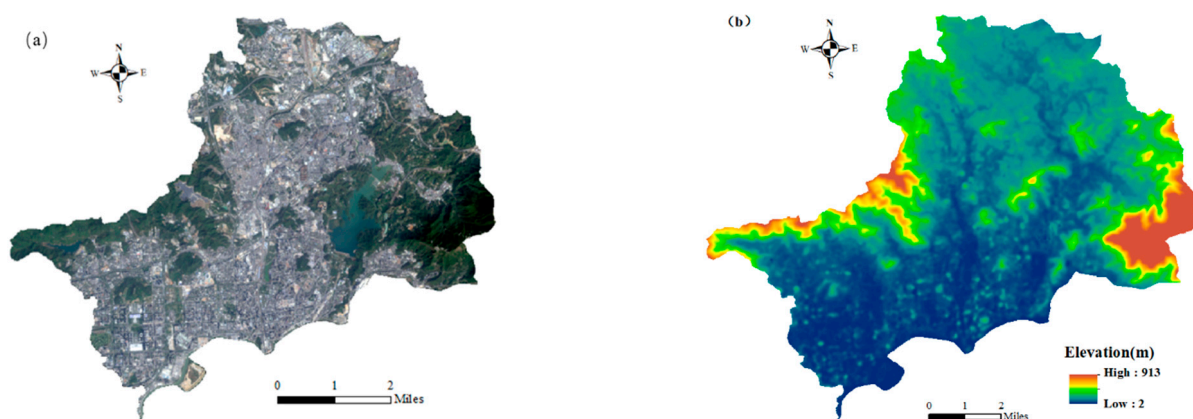


Figure 3. Cont.

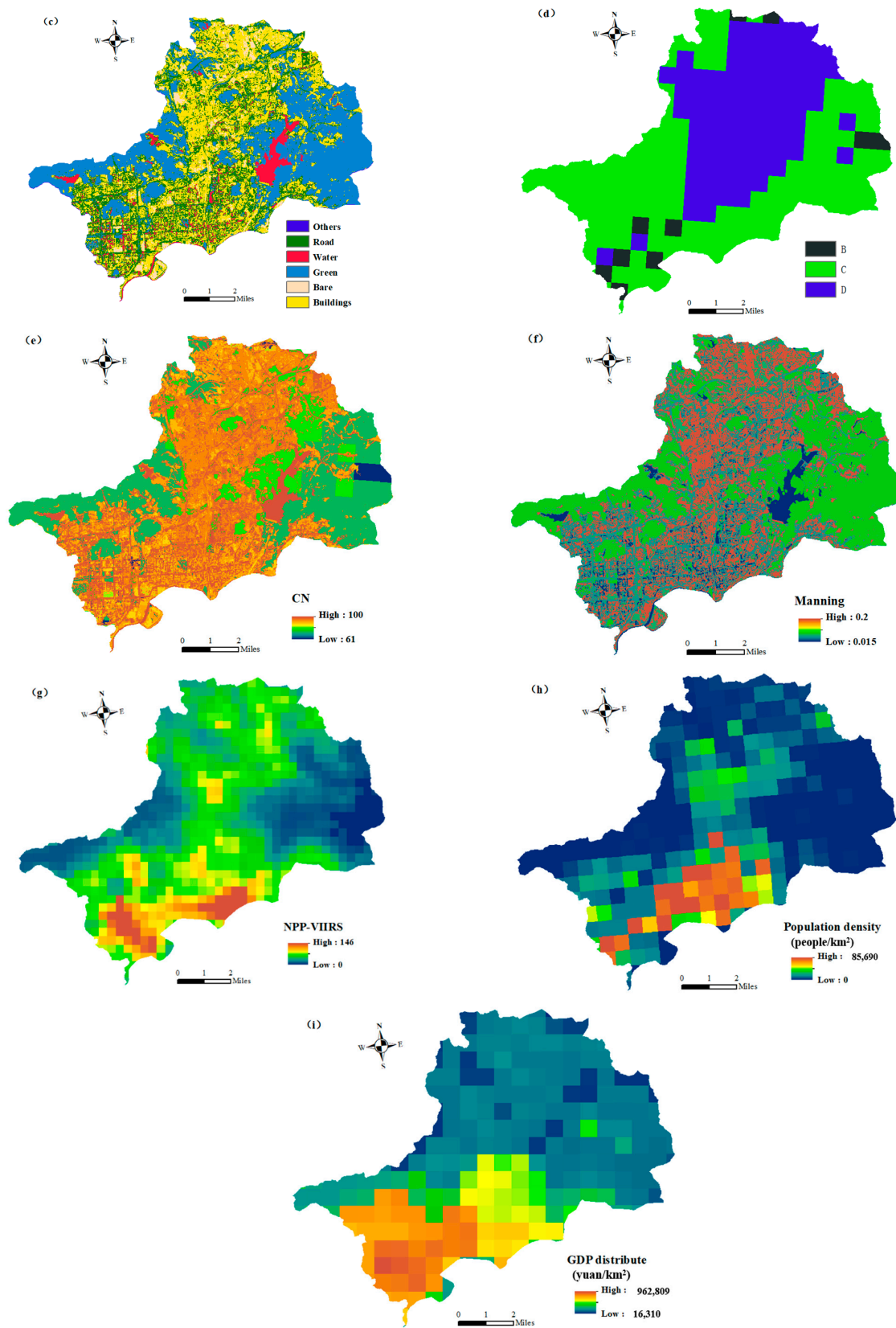


Figure 3. Condition of underlying surface: (a) remote sensing image, (b) elevation, m, (c) land use type, (d) soil classification, (e) CN value, (f) Manning coefficient, (g) NPP-VIIRS light data, (h) population density, people/km², (i) GDP distribute, yuan/km².

2.3. Design Rain Scenarios

In this study, by constructing an urban flood simulation model, different rainfall scenarios are designed to simulate and analyze the urban flood process in the study area. A total of 12 rainfall scenarios were set up, and the design rainstorm was calculated using the latest rainstorm intensity formula compiled by the Shenzhen Meteorological Bureau. The design formula of storm intensity is shown as Equation (9):

$$i = \frac{8.701(1 + 0.594\lg P)}{(t + 11.13)^{0.555}} \quad (9)$$

where i is the storm intensity(mm/min), P is the design return period(year), and t is rainfall duration (min).

Hyetographs of differently designed rainfall were determined using the Chicago Hydrograph Model commonly used in the world. The designed rainstorms had three return periods ($p = 20, 50$ and 100 years) and four rain peak coefficients ($r = 0.2, 0.4, 0.6$ and 0.8), the time interval was 1 min, and the rainfall duration was assumed as 120 min. In the process of surface two-dimensional flood simulation, because it is very difficult to obtain the pipeline network data in the study area, the underground pipeline network is generalized in this flood simulation. An equivalent drainage method is used to generalize the underground pipe network. Considering the adverse conditions such as aging, blockage and silting of the pipeline network, the drainage capacity of the pipeline network in the study area is 1-year rainfall scenario. The rainfall calculated according to the rainstorm intensity formula is used as the estimated amount of pipe network drainage, and this part of rainfall is equivalent to that deducted in the rainfall data and regarded as the rainfall discharged through the drainage pipe network. The designed rainstorm process obtained after synthesizing the rainfall process and the equivalent drainage effect of the pipe network is shown in Figure 4.

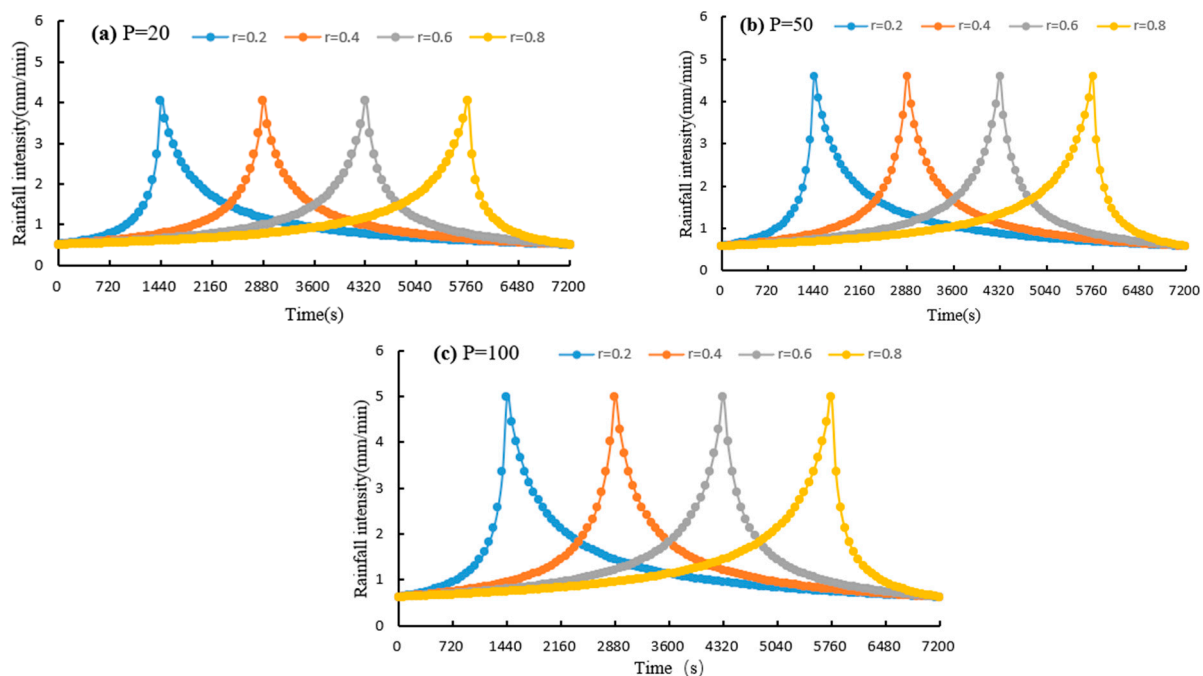


Figure 4. Synthetic hyetographs of the 12 design scenarios in the Shenzhen River Basin used in this study.

3. Results

3.1. Model Validation

Based on the TELEMAC-2D hydrodynamic model, the urban flood risk assessment in the SRB is carried out. In order to verify the accuracy and reliability of the model,

the measured rainfall data, the collection of waterlogged monitoring point data and the investigation of the actual inundation situation are selected to verify the accuracy of the model. After investigation and analysis, two measured rainfalls (7 June 2018 and 16 September 2018, Figure 5) were selected for simulation of the model, and the information on the actual waterlogged monitoring equipment in the study area was collected, with a total of 16 waterlogged monitoring points. The flooding process of the two rainfall events was simulated by the flood simulation model, and the inundation situation is shown in the Figure 6. The analysis shows that the actual waterlogging points are located in areas with high submerged water depth, and the simulation results are consistent with the actual situation, which proves that the established flood simulation model meets the requirements of accuracy and reliability. The actual submerged water depth data of some waterlogging points when the rainfall occurred was collected, and the data were compared with the numerical simulation results. It can be seen from Table 5 that the error between the submerged water depth obtained by the two actual rainfall simulations and the data of the submerged water depth obtained by the actual monitoring is small, which is basically controlled within 2 cm. The above two points show that the numerical simulation model established is relatively reliable in simulation accuracy and can be used for urban flood simulation in the study area.

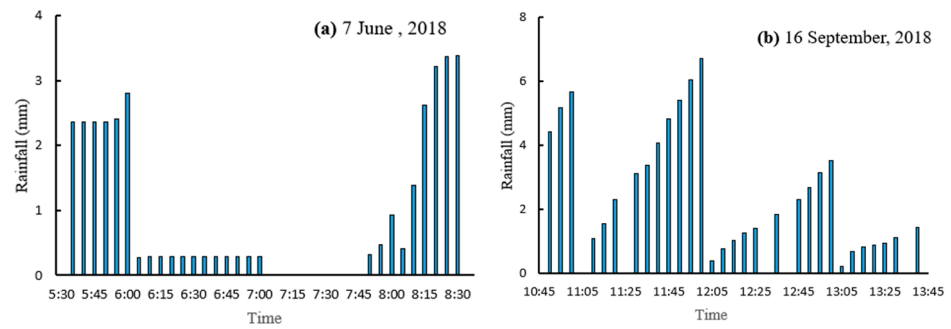


Figure 5. Rainfall processes of events on 7 June 2018 and 16 September 2018.

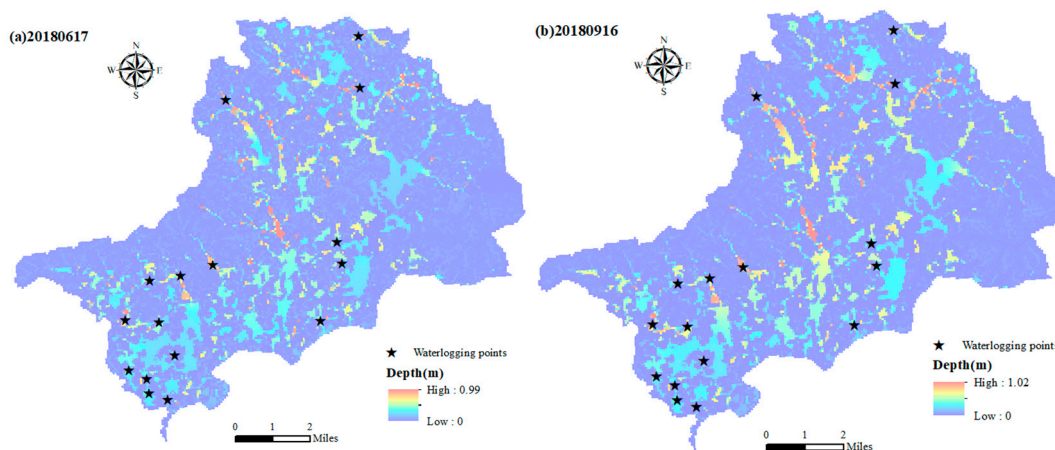


Figure 6. Measured rainfall inundation and location of waterlogging points.

Table 5. Maximum submerged water depth of waterlogging points.

Measured Rainfall	Number of Waterlogging Points	Measured Water Depth (cm)	Simulated Water Depth (cm)	Error (cm)
20180607	023	5	3	−2
	027	29	42.4	13.4
	074	2	3.2	1.2
	116	20	18.1	−1.9
	170	40	48	8
20180916	0.23	4	4.5	0.5
	116	14	13.9	−0.1
	121	20	17.8	−2.2
	122	2	2.6	−0.6

3.2. Analysis of Simulation Results

Based on the flood simulation model established by TELEMAC-2D two-dimensional hydrodynamic software, 12 design rainfall scenarios were simulated and calculated, and the inundation situation of the study area at the end of the simulation was obtained. The depth of inundation is one of the most important impact factors that should be considered when assessing flooding and the inundation of the entire study area is analyzed. Referring to the relevant literature, when the depth of inundation is greater than 0.15 m, there is a certain impact on road traffic; when the depth of inundation is greater than 0.3 m, it poses a hazard to the safety of people and generates more serious economic losses. The area when the inundation depth is greater than 0.15 m, 0.3 m and 0.5 m is calculated, respectively, in this paper, and the calculation results are shown in Table 6 and Figures 7 and 8. The analysis shows that with the increase in rainfall return period, the inundated area in the study area increases gradually. For the same rainfall return period, with the increase in the rain peak coefficient, the submerged area tends to increase. For example, when the return period is the 50-year rainfall scenario and the submerged water depth is greater than 0.5 m, the increase in the rain peak coefficient increased, and the submerged area was 19.73, 20, 20.732 and 21.641 hectares, respectively. When the return period is the 100-year rainfall scenario and the rain peak coefficient is 0.8, the area with submerged water depth >0.5 m is the largest, which is 0.74 km². When the return period is the 100-year rainfall scenario and the rain peak coefficient is 0.2, the area with submerged water depth >0.15 m is 5.37 km², which is the maximum submerged area;

Flood velocity is another important hazard factor in flood disasters. The flow rate of floods in the study area is mainly generated by gravity, so the flow rate and direction of water are closely related to the slope and elevation of the terrain, as shown in Table 7. With the increase of the rainfall return period, the maximum velocity increases gradually. In the case of the same rainfall return period, the maximum flow velocity values gradually increase as the rain peak coefficient increases. For example, in a 50-year flood scenario, the rain peak coefficient increases from 0.2 to 0.8, and the maximum flow velocities are 0.636, 0.652, 0.666 and 0.668 m/s, with relative increases of 2.03%, 2.15%, and 3.30% respectively. In the design scenario for this simulation, a maximum flow velocity of 0.765 m/s was obtained for the 100-year flood scenario when the rain peak coefficient was 0.8.

Table 6. Inundation area statistics under different rainfall scenarios.

Design Scenario		Area (10,000 m ²)		
		>0.15 m	>0.3 m	>0.5 m
r = 0.2	20a	108.161	22.676	3.931
	50a	319.162	91.363	19.73
	100a	531.901	226.641	73.745
		>0.15 m	>0.3 m	>0.5 m
r = 0.4	20a	109.263	24.102	4.064
	50a	319.527	89.959	20
	100a	531.91	228.919	71.296
		>0.15 m	>0.3 m	>0.5 m
r = 0.6	20a	110.265	24.623	4.083
	50a	320.41	90.396	20.732
	100a	533.744	233.845	68.495
		>0.15 m	>0.3 m	>0.5 m
r = 0.8	20a	113.467	24.834	4.095
	50a	321.956	90.908	21.641
	100a	537.239	238.401	67.493

Table 7. Maximum flood velocity statistics under different rainfall scenarios.

Design Scenario		Vmax (m/s)	Relative Growth
20a	r = 0.2	0.567	
	r = 0.4	0.584	3.00%
	r = 0.6	0.601	2.91%
	r = 0.8	0.624	3.83%
50a	r = 0.2	0.639	
	r = 0.4	0.652	2.03%
	r = 0.6	0.666	2.15%
	r = 0.8	0.688	3.30%
100a	r = 0.2	0.716	
	r = 0.4	0.728	1.68%
	r = 0.6	0.742	1.92%
	r = 0.8	0.765	3.10%

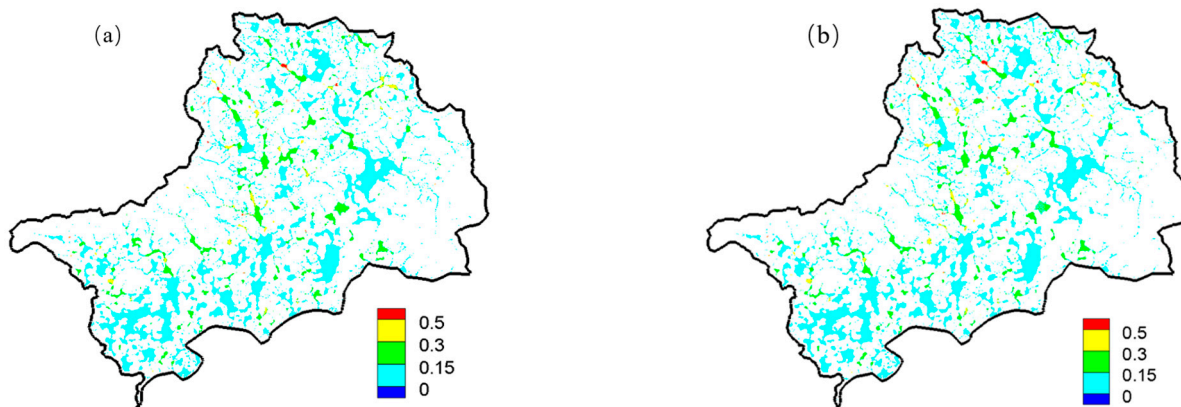


Figure 7. Cont.

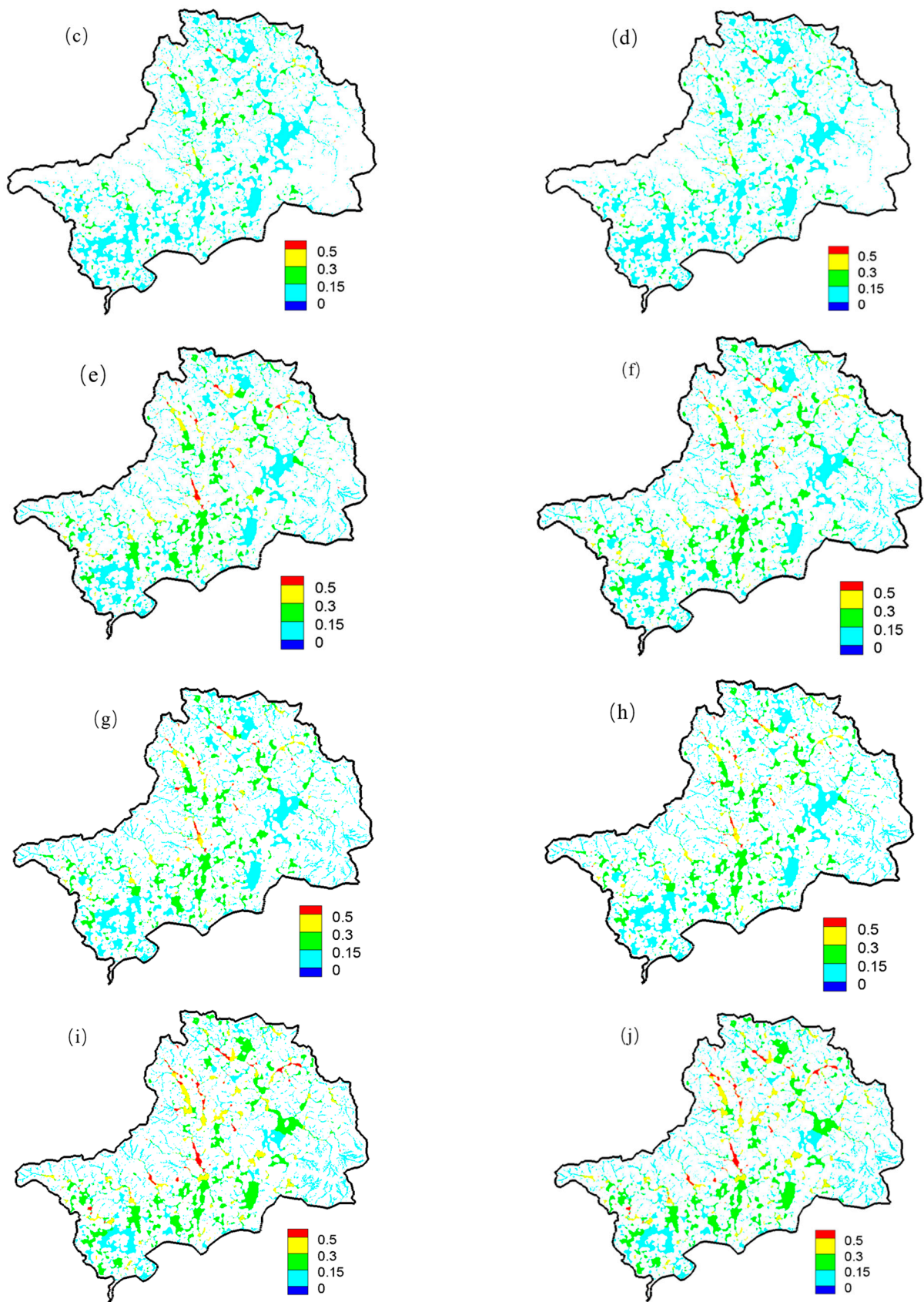


Figure 7. Cont.

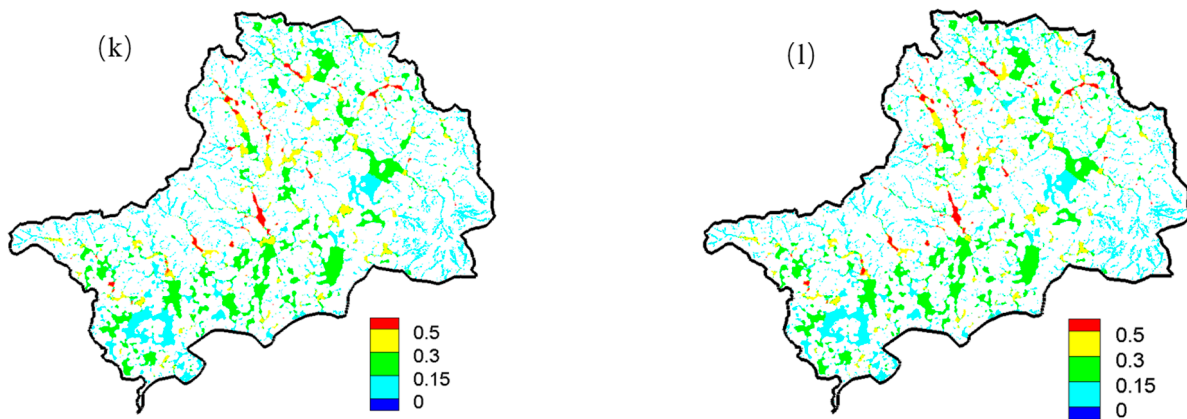


Figure 7. Inundation of Shenzhen River Basin in the Shenzhen River Basin (m): (a–d) $p = 20a$, $r = 0.2, 0.4, 0.6$ and 0.8 ; (e–h) $p = 50a$, $r = 0.2, 0.4, 0.6$ and 0.8 ; (i–l) $p = 100a$, $r = 0.2, 0.4, 0.6$ and 0.8 .

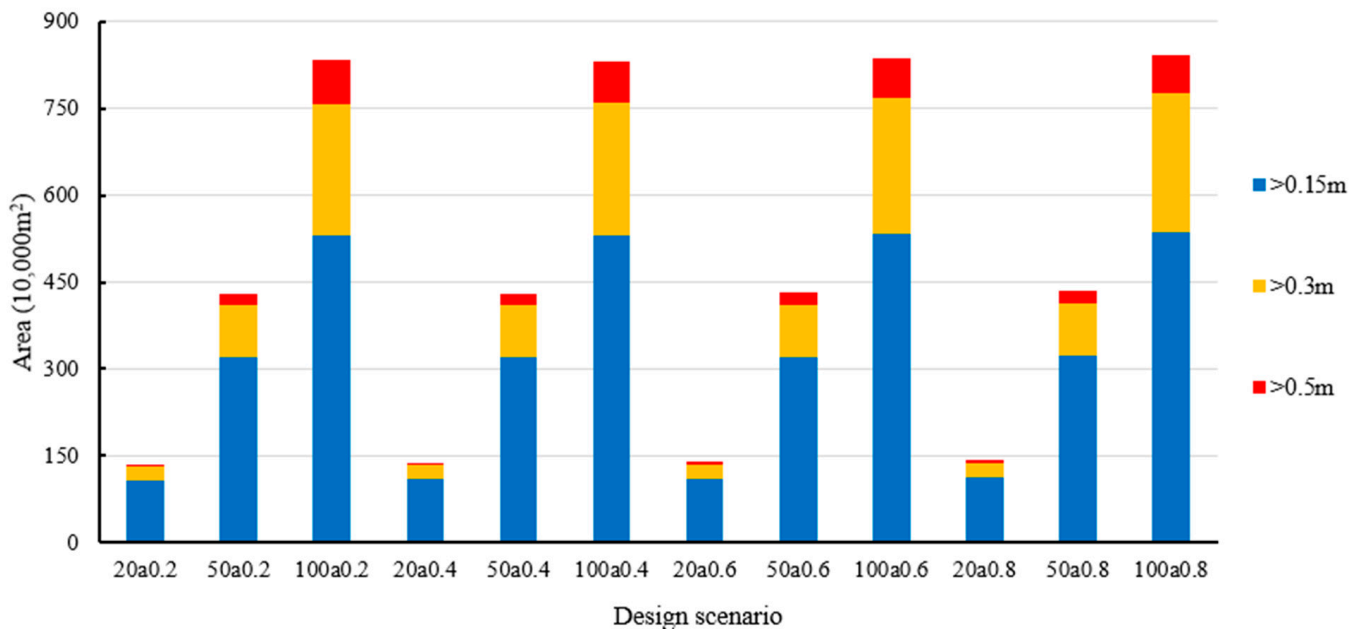


Figure 8. Inundation area map under different rainfall scenarios (20a0.4: rainfall return periods of 20 years and rainfall peak coefficients of 0.4).

3.3. Flood Disaster Risk Assessment

In this study, the H-V risk assessment method was used to assess the risk of urban flooding in the SRB. The hazard indicators considered include inundation depth, flow velocity, elevation and slope; vulnerability indicators include land use type, population density and property distribution. The weight value of each index was calculated based on the AHP method, the hazard and vulnerability index value of each grid unit was calculated by GIS, and the risk value of each grid unit was calculated according to the flood disaster risk expression formula. The flood risk distribution of the entire study area was obtained, and the calculated flood risk results were divided into four levels by using the natural discontinuity method: class I (highest risk), II (high risk), III (medium risk) and IV (least risk), represented by red, orange, yellow and blue, respectively. A flood risk zoning map under different rainfall scenarios is shown in Figure 9. In the SRB, the risk distribution of flood disasters is most affected by the inundation depth factor, followed by flood velocity and population density. The higher the above index factors, the higher the risk level of flood disasters.

The area and proportion of each risk area under different rainfall scenarios are counted, and the calculation results are shown in Table 8 and Figure 10. Analysis shows that under the 12 calculated rainfall scenarios, the class III area has the largest area, followed by the class IV area, and the class I area is the smallest. With the increase in the rainfall return period, the areas of highest-risk areas and high-risk areas increased, while the areas of medium-risk areas and least-risk areas decreased. As the rain peak coefficient gradually increased from 0.2 to 0.8, the area of each risk area increased, indicating that the larger the rain peak coefficient, the greater the risk of flooding in the study area. For instance, for a return period with a 20-year rainfall scenario, as the rain peak coefficient increases from 0.2 to 0.8, the highest-risk areas are 0.67, 0.68, 0.7 and 0.71 km² respectively. With increases in the rain peak coefficient, for the highest-risk areas, the area increases the fastest. For a return period of 20 years, as the rain peak coefficient increases from 0.2 to 0.8, the growth rate of the highest-risk areas is 1.49%, 2.94% and 1.43%. With the increase in the return period, the rain peak coefficient has no obvious effect on the area change of the highest-risk area. When the return period is 20 years, the rain peak coefficient has a greater impact on the area of risk area, especially for the highest-risk area, the area that has the fastest growth rate.

Table 8. Flood risk area statistics under different rainfall scenarios.

Designed Scenarios		Area (km ²)			
		I	II	III	IV
r = 0.2	20a	0.67	34.18	91.34	68.62
	50a	3.07	37.22	87.81	68.12
	100a	5.56	38.59	85.69	66.38
		I	II	III	IV
r = 0.4	20a	0.68	34.23	91.62	68.82
	50a	3.08	37.21	87.86	68.08
	100a	5.49	38.57	85.74	66.43
		I	II	III	IV
r = 0.6	20a	0.7	34.25	91.89	69.39
	50a	3.05	37.25	87.86	68.07
	100a	5.44	38.61	85.72	66.45
		I	II	III	IV
r = 0.8	20a	0.71	34.26	91.9	69.36
	50a	3.10	37.27	87.78	68.08
	100a	5.52	38.66	85.59	66.46

The SRB mainly includes LHD, FTD (part) and LGD (part), Shenzhen. When the rain peak coefficient is 0.4, the return period is 20, 50 and 100 years, respectively, to analyze the flood disaster risk zoning in different administrative areas, as shown in Table 9. With the increase in the return period, the areas of highest- and high-risk areas tended to increase, and the areas of highest-risk areas were 0.69, 3.07 and 5.49 km², respectively. The highest- and high-risk areas are mainly distributed in LHD, Shenzhen. The proportion of the highest-risk areas in LHD in Shenzhen and the high-risk areas in the basin is as follows. The proportion is 46.38% under the 20-year rainfall scenario, 60.91% under the 50-year rainfall scenario, and 38.28% under the 100-year rainfall scenario. The proportion of the high-risk area in LHD to Shenzhen and the high-risk area in the basin is as follows. Under the 20-year rainfall scenario, the proportion is 44.59%, in the 50-year rainfall scenario, the proportion is 40.64%, and in the 100-year rainfall scenario, the proportion is 66.4%. With the increase in the return period, although the area of highest-risk areas in FTD increases, its proportion has a

downward trend, and the proportion of highest-risk areas in LGD has an increasing trend. The terrain in LHD is flat, the population is concentrated, and the property distribution density is large. Once the flood disaster occurs, LHD will usually have a serious social impact and bring huge economic losses, so the risk of flood disaster is high.

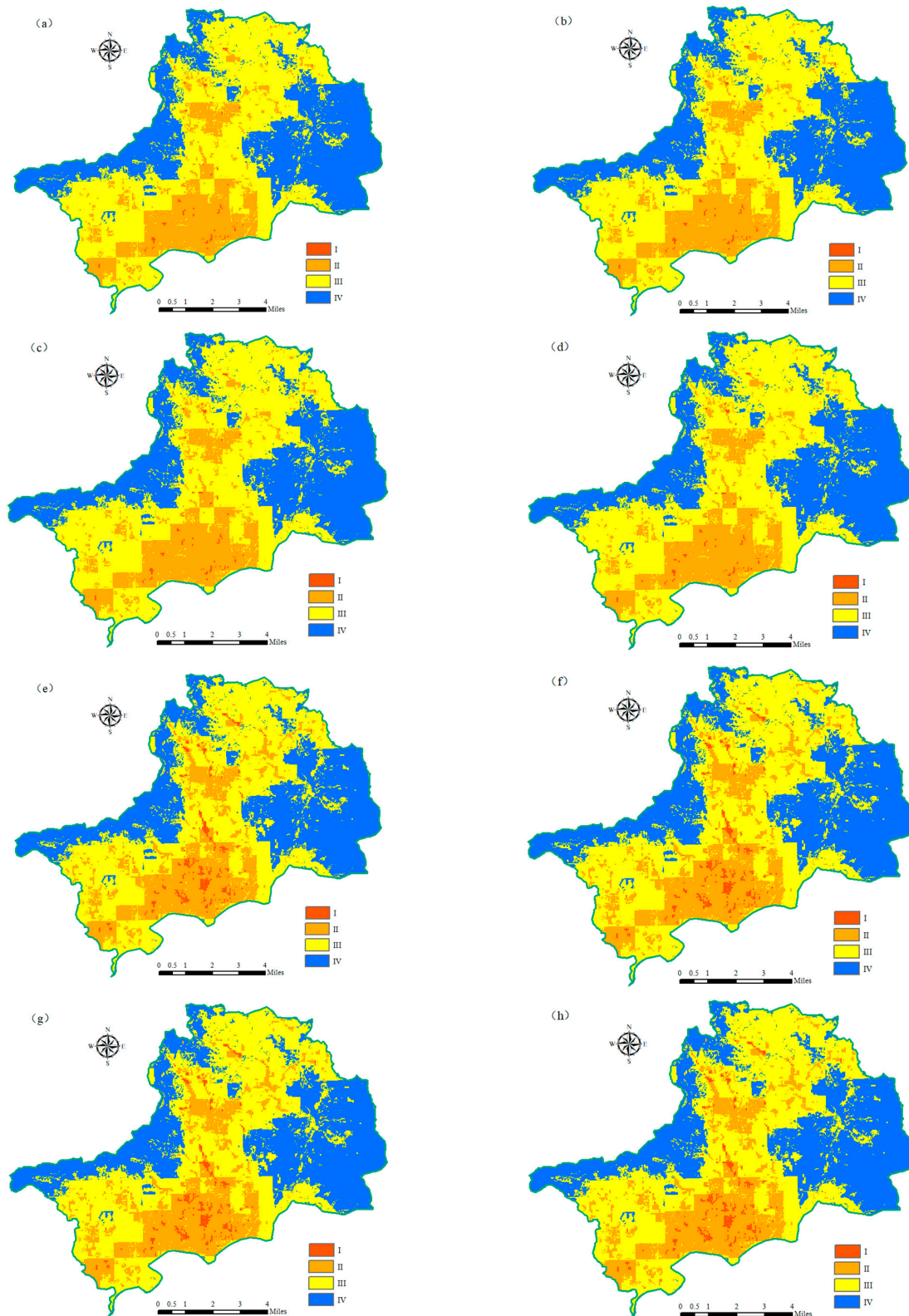


Figure 9. Cont.

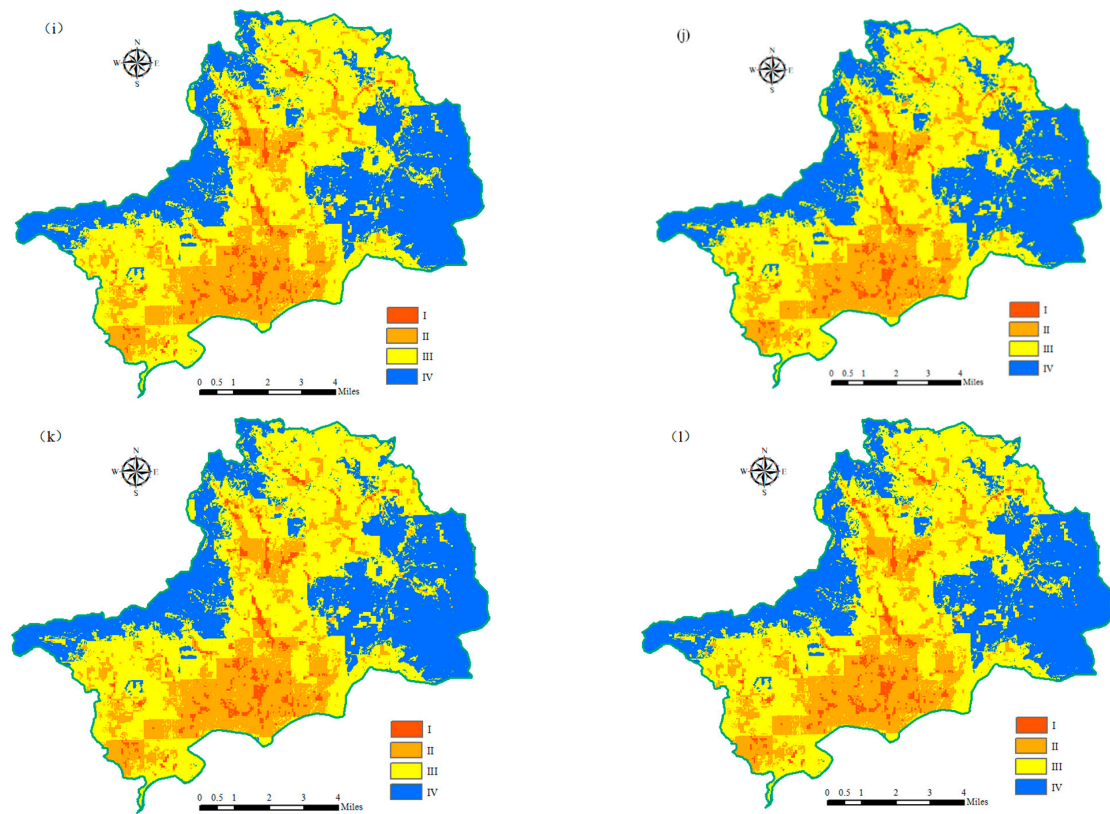


Figure 9. Flood risk zoning in the Shenzhen River Basin: (a–d) $p = 20a$, $r = 0.2, 0.4, 0.6$ and 0.8 ; (e–h) $p = 50a$, $r = 0.2, 0.4, 0.6$ and 0.8 ; (i–l) $p = 100a$, $r = 0.2, 0.4, 0.6$ and 0.8 . I: highest risk, II: high risk, III: medium risk and IV: least risk.

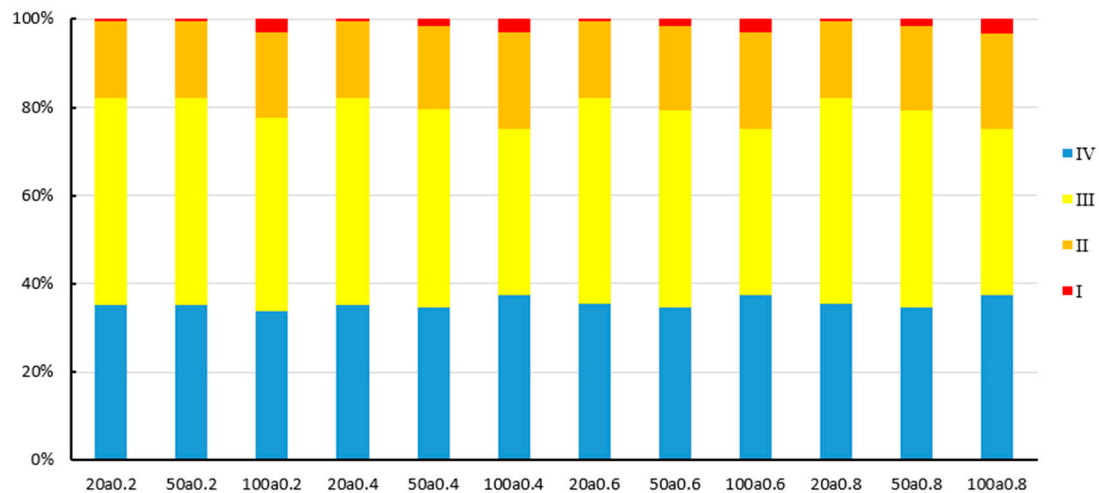


Figure 10. Percentage of risk areas under different rainfall scenarios. I: highest risk, II: high risk, III: medium risk and IV: least risk; (20a0.4: rainfall return periods of 20 years and rainfall peak coefficients of 0.4).

Table 9. The area of flood risk area under different administrative regions.

	District	Area (km ²)				Percentage (%)			
		I	II	III	IV	I	II	III	IV
20a0.4	LHD	0.32	15.26	23.31	40.41	46.38	44.59	25.45	59.4
	FTD	0.21	12.47	25.45	8.48	30.43	36.44	27.8	12.47
	LGD	0.16	6.49	42.8	19.14	23.19	18.97	46.75	28.13
	sum	0.69	34.22	91.56	68.03	1	1	1	1
50a0.4	LHD	1.87	15.13	22.68	33.64	60.92	40.64	25.82	59.04
	FTD	0.6	13.64	24.2	8.4	19.54	36.64	27.54	12.51
	LGD	0.6	8.46	40.97	19.1	19.54	22.72	46.64	28.45
	sum	3.07	37.23	87.85	67.14	1	1	1	1
100a0.4	LHD	2.5	45.54	22.98	38.28	45.54	66.4	26.81	58.45
	FTD	1.23	14.67	22.63	8.31	22.4	21.39	26.4	12.69
	LGD	1.76	8.37	40.11	18.9	32.06	12.2	46.79	28.86
	sum	5.49	68.58	85.72	65.49	1	1	1	1

4. Discussion

With climate change and increased urbanization, the frequency and intensity of extreme rainfall events have increased, leading to frequent urban flooding events [36–38]. Shenzhen city is located in the southeast coastal region of China, with abundant rainfall, and is hit by typhoons every year. Urban flooding events often occur. This paper selects the Shenzhen River Basin in Shenzhen as the study area, which includes Luohu District, Futian District (partly) and Longgang District (partly) and belongs to the economically developed and densely populated area of Shenzhen, while the topography of the study area is flat and surrounded by hills on three sides, which makes it highly susceptible to urban flooding. The results of the analysis show that as the rainfall peak coefficient factor increases, the area of each risk zone increases to varying degrees. The larger the rainfall peak coefficient factor, the more serious the flooding. As the rainfall return period increases, the effect of the rainfall peak coefficient factor on the change in the area of the highest risk zone diminishes. The highest risk zone is the largest within Luohu District (LHD), accounting for 46.38%, 60.92% and 45.54% of the total highest-risk area, respectively. As the return period increases, the area of the highest-risk zone within Futian District (FTD) increases, but its proportion has a decreasing trend, and the proportion of highest risk area within Longgang District (LGD) has an increasing trend. The article is of great significance in assessing the urban flood risk in the Shenzhen River Basin.

There are many methods for flood risk assessment, including hydrological and hydrodynamic methods [39], scenario simulation methods [30], GIS-based analysis methods [40–42], and machine learning-based methods [43,44]. A great deal of research has been carried out by scholars at home and abroad in the area of urban flood risk assessment, and fruitful results have been achieved [40,45–48]. Flood risk assessment methods are varied [49–51]. This paper proposes a novel approach to urban flood risk assessment based on the TELEMAC-2D two-dimensional hydrodynamic model for the simulation of urban flooding processes, coupled with natural geographic, social and economic distributions, to comprehensively assess urban flood risk levels. The method simulates the flooding process and extracts the inundation depth, flow velocity as well as elevation and slope factors from the simulation results as the causative factors while considering the commonly used H-V risk assessment method [52–54]. This study selects land use type, population density and GDP as vulnerability indicators and uses the powerful data processing function in ArcGIS for overlay analysis and classification to obtain an urban flood risk map of the Shenzhen River basin under the designed rainfall scenario.

The main advantage of this approach is that it takes into account multiple natural, social and economic indicators, simulates the urban flooding process based on the two-dimensional hydrodynamic model, and uses the powerful data analysis function of GIS to

realize the visualization of flood risk. The proposed method can be applied to other urban areas for flood analysis and assessment.

The application of this approach has some challenges. In the article, due to the difficulties in obtaining information on the underground drainage network in the study area, an equivalent drainage method was used to generalize the network during the flooding simulation, and there were certain errors in the flooding simulation results of this method, but the impact on the flood risk level assessment was small. The spatial resolution of the physical, social and economic distribution of information in the text varies from one source to another. In the text, the data are divided into the same size raster to make the results more reliable, and the spatial resolution of the indicator factors in subsequent studies should be the same so the analysis results will be more accurate. There are many factors affecting urban flood risk assessment, most of which change over time, such as rainfall intensity, rainfall volume, population density and property distribution, making it particularly difficult to build a unified urban flood risk assessment system. The current research mostly selects a few of the important indicators for analysis and assessment according to the selected study area. While there is also a large uncertainty in the determination of the weighting of each indicator factor, the size of the weighting has a large impact on the flood risk rating results, and the weighting should be determined objectively and carefully. Some scholars [55] study emergency rescue programs under heavy rainfall and flooding events. Analyzing and evaluating urban flooding can provide scientific references for urban emergency rescue programs, which is also the direction of future research [56].

5. Conclusions

Urban flood risk assessment and analysis is an important means of non-engineering measures in urban flood prevention and mitigation. In this paper, the SRB is used as the study area to carry out urban flood risk assessment work, and the main conclusions are as follows.

- (1) This paper proposes a method for urban flood risk assessment, which is based on the TLELMAC-2D two-dimensional hydrodynamic model for urban flood simulation and coupled with multi-index factors such as natural geographical conditions and social and economic conditions to assess urban flood risk and is able to give urban flood risk assessment results with a spatial resolution of 30 m. The accuracy and reliability of the method have been verified in the Shenzhen River basin, and the results are reliable. The method can also be used in other research areas for urban flood risk analysis, providing a scientific basis for urban disaster prevention and mitigation early warning.
- (2) Based on the TELEMAC-2D two-dimensional hydrodynamic model, an urban flood simulation model was constructed, and the equivalent drainage method was used to generalize the drainage capacity of the urban underground pipe network. The accuracy and reliability of the model were verified by using two measured rainfall data. The results show that the established model has good accuracy and reliability and can be used to simulate flooding processes in the study area and obtain the disaster-causing factors of urban floods;
- (3) The H-V method was used to assess the flood risk in the SRB, and a total of seven index evaluation factors were selected: inundation depth, flood velocity, elevation, slope, land use type, population density and property distribution. The AHP method was used to determine the weight values of each index factor, and the natural interruption method and threshold division were used to carry out overlay analysis in ArcGIS to draw an urban flood risk zoning map for the SRB under different design rainfall scenarios.
- (4) Inundation depth is the most important influencing factor for flooding in the SRB, followed by flood flow velocity and population density. The greater the depth of inundation, the faster the flow velocity and the more concentrated the population distribution; thus, the more severe the flooding situation. With the increase in the rain peak coefficient, the area of each risk area increased to different degrees, indicating

that the larger the rain peak coefficient, the more serious the flood disaster. As the rain peak coefficient increased, the area of highest-risk areas increased the fastest. In the 20 years rainfall scenario, as the rain peak coefficient increases from 0.2 to 0.8, the growth rates of highest-risk areas are 1.49%, 2.94% and 1.43%. As the rainfall return period increases, the effect of the rain peak coefficient on the change in the area of the highest risk zone diminishes.

- (5) An analysis of the distribution of flood risk levels within different administrative areas of the SRB under three scenarios with a rain peak coefficient of 0.4 and rainfall return periods of 20, 50 and 100 years is conducted. Within the LHD, the highest-risk area is the largest and accounts for the largest proportion of the total highest-risk area, at 46.38%, 60.92% and 45.54%, respectively. As the return period increases, the area of highest-risk areas within FTD increases, but its proportion tends to decrease, and the proportion of highest-risk areas within LGD tends to increase. The flood risk zoning map made in this study can better reflect the actual inundation situation in the study area and can provide a reference basis for urban flood control and drainage decisions in the SRB.

Author Contributions: Conceptualization, G.L. and J.L.; methodology, G.L. and J.L.; software, G.L.; validation, G.L. and J.L.; formal analysis, G.L.; investigation, G.L.; resources, G.L. and J.L.; data curation, G.L.; writing—original draft preparation, G.L.; writing—review and editing, G.L.; visualization, G.L.; supervision, G.L.; project administration, J.L.; funding acquisition, J.L. and W.S. All authors have read and agreed to the published version of the manuscript.

Funding: This study was supported by the Chinese National Natural Science Foundation (No. 51979285 and 51739011), and the Research Fund of the State Key Laboratory of Simulation and Regulation of Water Cycle in River Basin (SKL2022TS11).

Institutional Review Board Statement: Not applicable.

Informed Consent Statement: Not applicable.

Data Availability Statement: The datasets used and analyzed during the current study are available from the corresponding authors upon reasonable request.

Conflicts of Interest: The authors declare no conflict of interest.

References

1. Wesley, W.; Mohammad, M.; Maziar, Y.; Kamyar, K. The Alignment of Australia's National Construction Code and the Sendai Framework for Disaster Risk Reduction in Achieving Resilient Buildings and Communities. *J. Build.* **2021**, *11*, 429. [CrossRef]
2. Haasnoot, M.; Middelkoop, H.; Offermans, A.; Beek, E.V.; Deursen, W.J. Exploring pathways for sustainable water management in river deltas in a changing environment. *Clim. Chang.* **2012**, *115*, 795–819. [CrossRef]
3. Adolfo, Q.-R. Flood risk index development at the municipal level in Costa Rica: A methodological framework. *Environ. Sci. Policy* **2022**, *133*, 98–106. [CrossRef]
4. Winsemius, H.C.; Aerts, J.C.J.H.; van Beek, L.P.H.; Bierkens, M.F.P.; Bouwman, A.; Jongman, B.; Kwadijk, J.C.J.; Ligtvoet, W.; Lucas, P.L.; van Vuuren, D.P.; et al. Global drivers of future river flood risk. *J. Nat. Clim. Chang.* **2016**, *6*, 381–385. [CrossRef]
5. Aerts, J.C.J.H.; Botzen, W.J.; Clarke, K.C.; Cutter, S.L.; Hall, J.W.; Merz, B.; Michel-Kerjan, E.; Mysiak, J.; Surminski, S.; Kunreuther, H. Integrating human behaviour dynamics into flood disaster risk assessment. *J. Nat. Clim. Chang.* **2018**, *8*, 193–199. [CrossRef]
6. Yuehua, Z.; Tao, P.; Ruiqin, S. Research progress on risk assessment of heavy rainfall and flood disasters in China. *Torrential Rain Disasters* **2019**, *38*, 494–501.
7. Junfei, C.; Jiamin, D.; Menghua, D. Research Progress on Risk Assessment and Management for Urban Stormwater. *J. Catastrophol.* **2020**, *35*, 154–159, 166. [CrossRef]
8. Carraro, C.; Lanza, A.; Tavoni, M. All You Need to Know about the IPCC 5th Assessment Report. Mitigation of Climate Change. In *Review of Environment, Energy and Economics—Re3*; 2014; Available online: <https://ideas.repec.org/a/fem/femre3/2014.04-03.html> (accessed on 10 July 2022).
9. National Bureau of Statistics of China. *Statistical Bulletin of the People's Republic of China on National Economic and Social Development in 2019*; China statistics; National Bureau of Statistics of China: Beijing, China, February 2020. Available online: http://www.gov.cn/xinwen/2020-02/28/content_5484361.htm (accessed on 10 July 2022).
10. Guoru, H.; Xin, W.; Wei, H. Simulation of Rainstorm Water Logging in Urban Area Based on InfoWorks ICM Model. *Water Resour. Power* **2017**, *35*, 66–70+60.

11. Zhang, J.; Wang, Y.; He, R.; Hu, Q.; Song, X. Discussion on the urban flood and waterlogging and causes analysis in China. *Adv. Water Sci.* **2016**, *27*, 7. [CrossRef]
12. Islam, A.R.M.T.; Talukdar, S.; Mahato, S.; Kundu, S.; Eibek, K.U.; Pham, Q.B.; Kuriqi, A.; Linh, N.T.T. Flood susceptibility modelling using advanced ensemble machine learning models. *Geosci. Front.* **2021**, *12*, 101075. [CrossRef]
13. Zhang, D.; Shi, X.; Xu, H.; Jing, Q.; Pan, X.; Liu, T.; Wang, H.; Hou, H. A GIS-based spatial multi-index model for flood risk assessment in the Yangtze River Basin, China. *Environ. Impact Assess. Rev.* **2020**, *83*, 106397. [CrossRef]
14. Mishra, K.; Sinha, R. Flood risk assessment in the Kosi megafan using multi-criteria decision analysis: A hydro-geomorphic approach. *Geomorphology* **2020**, *350*, 106861. [CrossRef]
15. Lei, X.; Chen, W.; Panahi, M.; Falah, F.; Rahmiti, O.; Uuemaa, E.; Kalantari, Z.; Ferreira, C.S.S.; Rezaie, F.; Tiefenbacher, J.P.; et al. Urban flood modeling using deep-learning approaches in Seoul, South Korea. *J. Hydrol.* **2021**, *601*, 126684. [CrossRef]
16. Tomar, P.; Singh, S.K.; Kanga, S.; Meraj, G.; Kranji, N.; Urin, B.; Pattanaik, A.J.S. GIS-Based Urban Flood Risk Assessment and Management—A Case Study of Delhi National Capital Territory (NCT), India. *Sustainability* **2021**, *13*, 12850. [CrossRef]
17. Chen, X.; Zhang, H.; Chen, W.; Huang, G. Urbanization and climate change impacts on future flood risk in the Pearl River Delta under shared socioeconomic pathways. *Sci. Total Environ.* **2020**, *762*, 143144. [CrossRef]
18. Salman, A.M.; Li, Y. Flood Risk Assessment, Future Trend Modeling, and Risk Communication: A Review of Ongoing Research. *Nat. Hazards Rev.* **2018**, *19*. [CrossRef]
19. Jiahong, L.; Zhouan, L.; Yongxiang, Z.; Jinjun, Z.; Weiwei, S. Influence of urbanization on spatial distribution of extreme precipitation in Henan Province. *Water Resour. Prot.* **2022**, *38*, 100–105.
20. Jiahong, L.; Xiangyi, D.; Weiwei, S.; Zhiyong, Y.; Chao, M. Characteristics of total runoff control rate of sponge cities for different hydrological year types. *J. Hydraul. Eng.* **2019**, *50*, 1072–1077. [CrossRef]
21. Yashon, O.; Ryutaro, T.J.W. Urban Flood Vulnerability and Risk Mapping Using Integrated Multi-Parametric AHP and GIS: Methodological Overview and Case Study Assessment. *Water* **2014**, *6*, 1515–1545.
22. Jiahong, L.; Jia, W.; Hao, W.; Chao, M. Effectiveness of urban inundation control system in sponge city construction. *Adv. Water Sci.* **2020**, *31*, 611–618. [CrossRef]
23. Pham, B.T.; Luu, C.; Van Dao, D.; Phong, T.V.; Nguyen, H.D.; Van Le, H.; von Meding, J.; Prakash, I. Flood risk assessment using deep learning integrated with multi-criteria decision analysis. *Knowl. Based Syst.* **2021**, *219*, 106899. [CrossRef]
24. Pham, B.T.; Luu, C.; Phong, T.V.; Nguyen, H.D.; Prakash, I. Flood risk assessment using hybrid artificial intelligence models integrated with multi-criteria decision analysis in Quang Nam Province, Vietnam. *J. Hydrol.* **2021**, *592*, 125815. [CrossRef]
25. Budiyo, Y.; Aerts, J.; Brinkman, J.J.; Marfai, M.A.; Ward, P. Flood risk assessment for delta mega-cities: A case study of Jakarta. *Nat. Hazards* **2015**, *75*, 389–413. [CrossRef]
26. Foudi, S.; Osés-Eraso, N.; Tamayo, I. Integrated spatial flood risk assessment: The case of Zaragoza. *Land Use Policy* **2015**, *42*, 278–292. [CrossRef]
27. Li, Z.; Song, K.; Peng, L. Flood Risk Assessment under Land Use and Climate Change in Wuhan City of the Yangtze River Basin, China. *Land* **2021**, *10*, 878. [CrossRef]
28. Guoru, H.; Haiwan, L.; Xinxiang, L.; Conghui, Y.; Zheng, W.; Ting, H.; Jingguang, M. Study on risk analysis and zoning method of urban flood disaster. *Water Resour. Prot.* **2020**, *36*, 7. [CrossRef]
29. Xin, S.; Weiwei, S.; Jiahong, L.; Yunzhong, J.; Kaibo, W. Dynamic Assessment of the Impact of Flood Disaster on Economy and Population under Extreme Rainstorm Events. *Remote Sens.* **2021**, *13*, 3924. [CrossRef]
30. Baky, M.; Islam, M.; Paul, S.J. Flood Hazard, Vulnerability and Risk Assessment for Different Land Use Classes Using a Flow Model. *Earth Syst. Environ.* **2020**, *4*, 225–244. [CrossRef]
31. Penggen, C.; Yin, H. Flood risk assessment of Nanchang City based on AHP and Entropy Method. *Yangtze River* **2021**, *52*, 8.
32. Saaty, T.L. A scaling method for priorities in hierarchical structures. *J. Math. Psychol.* **2000**, *15*, 234–281. [CrossRef]
33. Kazakis, N.; Kougias, I.; Patsialis, T. Assessment of flood hazard areas at a regional scale using an index-based approach and Analytical Hierarchy Process: Application in Rhodope–Evros region, Greece. *Sci. Total Environ.* **2015**, *538*, 555–563. [CrossRef] [PubMed]
34. Yiheng, X.; Chunxia, Y.; Yiyao, L.; Yuequn, L.; Xiaoyue, Z.; Qitang, H. Relationship between Landscape Pattern and Surface Runoff in Fuzhou Based on GIS. *Water Resour. Power* **2017**, *5*. Available online: http://en.cnki.com.cn/Article_en/CJFDTOTAL-SDNY201706004.htm (accessed on 10 July 2022).
35. Jiahong, L.; Zejin, L.; Chao, M.; Kaibo, W.; Guannan, Z. Urban flood analysis for different design storm hyetographs in Xiamen Island based on TELEMAC-2D. *Chin. Sci. Bull.* **2019**, *64*, 2055–2066.
36. Bera, A.; Taloor, A.; Meraj, G.; Kanga, S.; Singh, S.K.; Durin, B.; Anand, S. Climate vulnerability and economic determinants: Linkages and risk reduction in Sagar Island, India; A geospatial approach. *Quat. Sci. Adv.* **2021**, *4*, 100038. [CrossRef]
37. Camorani, G.; Castellarin, A.; Brath, A. Effects of land-use changes on the hydrologic response of reclamation systems. *Phys. Chem. Earth Parts A/B/C* **2005**, *30*, 561–574. [CrossRef]
38. Halgamuge, M.N.; Nirmalathas, A. Analysis of Large Flood Events: Based on Flood Data During 1985–2016 in Australia and India. *Int. J. Disaster Risk Reduct.* **2017**, *24*, S2212420916308056. [CrossRef]
39. Gharbi, M.; Soualmia, A.; Dartus, D.; Masbernati, L. Comparison of 1D and 2D hydraulic models for floods simulation on the medjerda river in Tunisia. *J. Mater. Environ. Sci.* **2016**, *7*, 3017–3026.

40. Waghwal, R.K.; Agnihotri, P.G. Flood risk assessment and resilience strategies for flood risk management: A case study of Surat City. *Int. J. Disaster Risk Reduct.* **2019**, *40*, 101155. [[CrossRef](#)]
41. Qra, B.; Bca, C.; Gb, B.; Cb, B.; Msac, D.J.G. Improving regional flood risk assessment using flood frequency and dendrogeomorphic analyses in mountain catchments impacted by tropical cyclones. *Geomorphology* **2022**, *396*, 108000. [[CrossRef](#)]
42. Quesada-Román, A.; Villalobos-Chacón, A. Flash flood impacts of Hurricane Otto and hydrometeorological risk mapping in Costa Rica. *Geogr. Tidsskr. Dan. J. Geogr.* **2020**, *120*, 1822195. [[CrossRef](#)]
43. Khan, T.A.; Shahid, Z.; Alam, M.; Su'ud, M.M.; Kadir, K. Early Flood Risk Assessment using Machine Learning: A Comparative study of SVM, Q-SVM, K-NN and LDA. In Proceedings of the 2019 13th International Conference on Mathematics, Actuarial Science, Computer Science and Statistics (MACS), Karachi, Pakistan, 14–15 December 2019.
44. Chen, J.; Huang, G.; Chen, W. Towards better flood risk management: Assessing flood risk and investigating the potential mechanism based on machine learning models. *J. Environ. Manag.* **2021**, *293*, 112810. [[CrossRef](#)] [[PubMed](#)]
45. Fariza, A.; Basofi, A.; Prasetyaningrum, I.; Pratiwi, V.I. Urban Flood Risk Assessment in Sidoarjo, Indonesia, Using Fuzzy Multi-Criteria Decision Making. *J. Phys. Conf. Ser.* **2020**, *1444*, 012027. [[CrossRef](#)]
46. Hosseinzadehtalaei, P.; Ishadi, N.K.; Tabari, H.; Willems, P. Climate change impact assessment on pluvial flooding using a distribution-based bias correction of regional climate model simulations. *J. Hydrol.* **2021**, *598*, 126239. [[CrossRef](#)]
47. Tabari, H.; Asr, N.M.; Willems, P. Developing a framework for attribution analysis of urban pluvial flooding to human-induced climate impacts. *J. Hydrol.* **2021**, *598*, 126352. [[CrossRef](#)]
48. Ferguson, C.; Fenner, R. The impact of Natural Flood Management on the performance of surface drainage systems: A case study in the Calder Valley. *J. Hydrol.* **2020**, *590*, 125354. [[CrossRef](#)]
49. Lee, G.; Jun, K.-S.; Chung, E.-S. Integrated multi-criteria flood vulnerability approach using fuzzy TOPSIS and Delphi technique. *Nat. Hazards Earth Syst. Sci.* **2013**, *13*, 1293–1312. [[CrossRef](#)]
50. Winsemius, H.C.; Beek, L.P.H.V.; Jongman, B.; Ward, P.J.; Bouwman, A. A framework for global river flood risk assessments. *Hydrol. Earth Syst. Sci.* **2013**, *17*, 1871–1892. [[CrossRef](#)]
51. Brenden, J.; Ward, P.J.; Aerts, J.C.J.H. Global exposure to river and coastal flooding: Long term trends and changes. *Glob. Environ. Change* **2012**, *22*, 823–835. [[CrossRef](#)]
52. Huang, G.R.; Xian, Z.Y.; Cheng, G.D.; Chen, Z.L.; Zhou, X.M. Risk Assessment of Mountain Torrent Disaster at Yaoan Small Watershed in Qingyuan City Based on GIS Technique. *J.W.R. Power* **2015**, *33*, 43–47.
53. Luo, H.; Chen, W.; Zhiwei, L.L.; Pan, J.; Gao, Q.; Huang, G.; School of Civil Engineering and Transportation, South China University of Technology; Guangzhou Water Science Research Institute; State Key Laboratory of Subtropical Building Science, South China University of Technology; Guangdong Engineering Technology Research Center of Safety and Greenization for Water Conservancy Project. Flood simulation of Donghaochong Basin in Guangzhou City based on coupled hydrodynamic model. *J. Water Resour. Water Eng.* **2019**, *3*, 46–52.
54. Park, K.; Won, J.-H. Analysis on distribution characteristics of building use with risk zone classification based on urban flood risk assessment. *Int. J. Disaster Risk Reduct.* **2019**, *38*, 101192. [[CrossRef](#)]
55. Yazdani, M.; Mojtahedi, M.; Loosemore, M.; Sanderson, D. A modelling framework to design an evacuation support system for healthcare infrastructures in response to major flood events. *Prog. Disaster Sci.* **2022**, *13*, 100218. [[CrossRef](#)]
56. Tong, J.; Zhang, H.; Liu, H.; Huang, J.; Hao, Y. XGBoost model-based risk assessment and influencing factors analysis of waterlogging in core cities of Yangtze River Delta. *Water Resour. Hydropower Eng.* **2021**, *52*, 1–11. [[CrossRef](#)]